Electronic Supplementary Material (ESI) for Sustainable Energy & Fuels.

Supplementary materials

Translating Local Binding Energy to a Device Effective one

Dan Liraz,[1] Pei Cheng,[2] Yang Yang,[2] Nir Tessler[1]

[1] *Microelectronic & Nanoelectronic Centers, Electrical Engineering Department, Technion Israel Institute of Technology, Haifa (Israel)*
2 *Department of Materials Science and Engineering, University of California, Los Angeles, CA, USA*

1. Calculating Ω(r)

Our method of counting is described in the paper. In this section, we give some counting result for different morphologies.

2. Morphology/Geometry

First, we describe the simplest morphology. Consider a symmetrical (the morphology of donor and acceptor is identical), device, with cubic lattice, with lattice parameter of 1[nm]. The 2D analog situation is shown in Figure 1S. Point '*j*' is located at the origin. The colored area represents sites which are part of r-separated pair-configuration. Note that a colored site may participate in multiple r-separated pair-configuration.

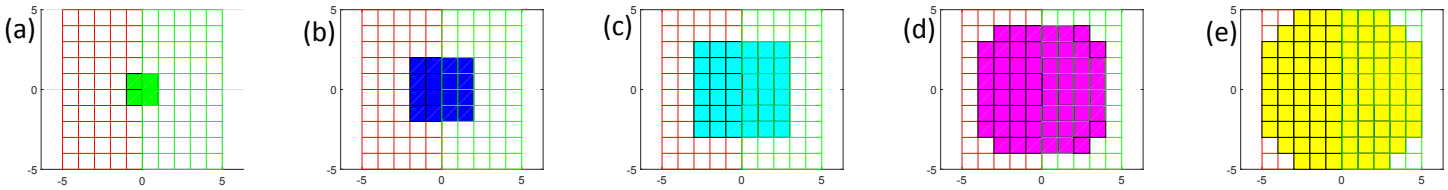

Figure 1S. 2D illustration of simple morphology. Red mesh describes sites on side A and green mesh – side B. Point 'j' is located at the origin. The colored area represents sites which taking place in forming r-separated CT. graphs (a)-(e) present the feeding area for r-separated CTs, where r is equal to 1-5[nm] respectively

Second, replace one side cubic lattice with elongated shaped sites, 'face-on' conformation, represented by 1X4X1 cuboid. we use Cartesian coordinate system (x, y, z), when the x-axis is perpendicular to donor-acceptor interface and y, z axes are parallel to it. The 2D analog situation is shown in Figure 2S.

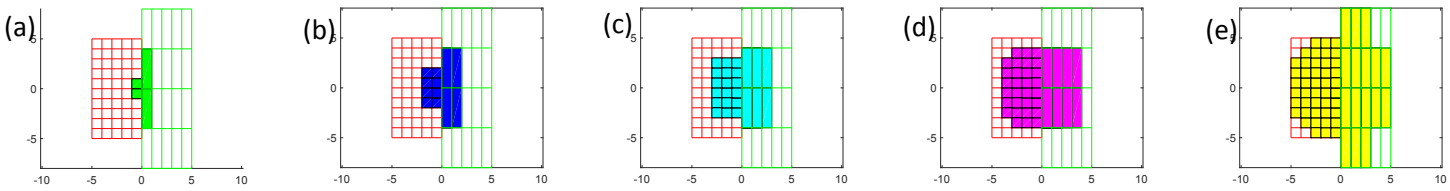

Figure 2S. 2D illustration of sites with elongated shape morphology, 'face-on' conformation (compare to Figure 1S).

Third, similar to second case, but instead consider ‘edge-on’ conformation. 2D analog situation is shown in Figure 3S.

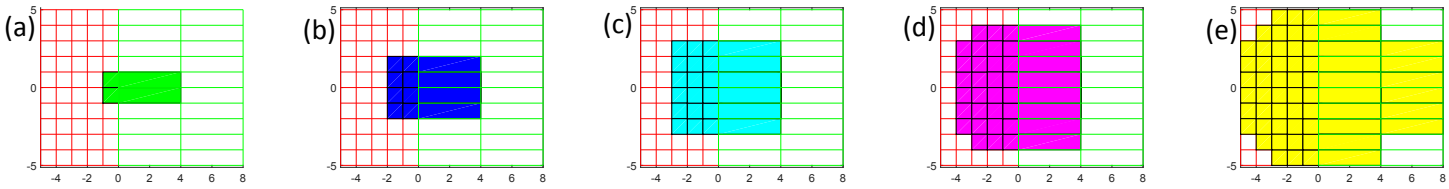

Figure 3S. 2D illustration of sites with elongated shape morphology, ‘edge-on’ conformation (compare to Figure 2S and Figure 1S).

Fourth, examine more elongated (1X10X1) ‘face-on’ system.

Fifth is a parallel ‘face-on’:’face-on’ system represented by 1X10X1:1X10X1 cuboids (Figure 4S).

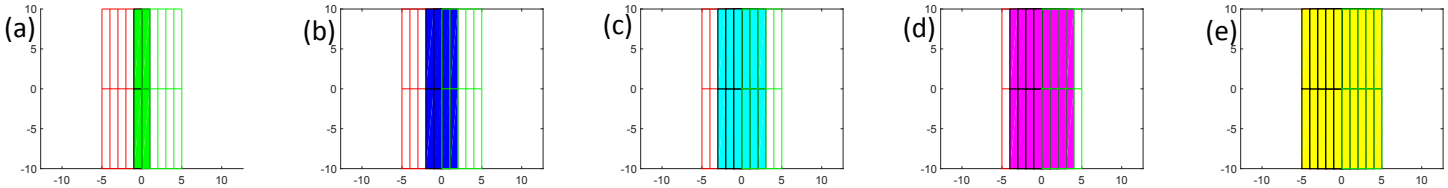

Figure 4S. 2D illustration parallel ‘face-on’:’face-on’ system (compare to Figure 1S).

Sixth is a perpendicular ‘face-on’:’face-on’ system represented by 1X10X1:1X1X10 cuboids (Figure 5S).

Figure 5S. 3D illustration of a perpendicular ‘face-on’:’face-on’ system (compare to *Figure* 4S).

Seventh is a ‘face-on’:’edge-on’ system represented by 1X10X1:10X1X1 cuboids

Eighth is a 1X1X1:3X3X3 system.

Ninth is a 1X6X10:3X3X3 system.

For each morphology, we calculated Ω as a function of r and extracted its figure of merit. Table 1S organizes the counting results.

Number	dimensions	Figure of merit	a	R^3
1	1X1X1:1X1X1	$a \cdot r^3$	2.27±0.03	0.999
2	1X1X1:1X4X1	$a \cdot r^3$	1.94±0.02	0.999
3	1X1X1:4X1X1	$a \cdot r^3$	1.94±0.02	0.999
4	1X1X1:1X10X1	$a \cdot r^3$	1.89±0.01	1.000
5	1X10X1: 1X10X1	$a \cdot r^3$	1.39±0.01	1.000
6	1X10X1: 1X1X10	$a \cdot r^3$	1.40±0.01	1.000
7	1X10X1: 10X1X1	$a \cdot r^3$	1.40±0.01	1.000
8	1X1X1:3X3X3	$a \cdot r^3$	1.52±0.01	1.000
9	1X6X10:3X3X3	$a \cdot r^3$	0.73±0.02	0.995

Table 1S. counting Ω(r) for diverse morphology

We conclude, that although the result is always proportional to r^3, the pre-factor may change by a factor of up to three depending on the morphology.

3. Ordered interfacial layer

We simulated the case when the first interfacial layers of the donor and acceptor are ordered. All other molecules are energetic disordered with Gaussian distribution, the width of this distribution is according to the graph legend. We apply the EED model on a cubic geometry with lattice constant of 1 nm and assume ε=3.3.

Compare these narrow local binding energy distributions to the results of the fully disordered system (Figure 4 a and b).

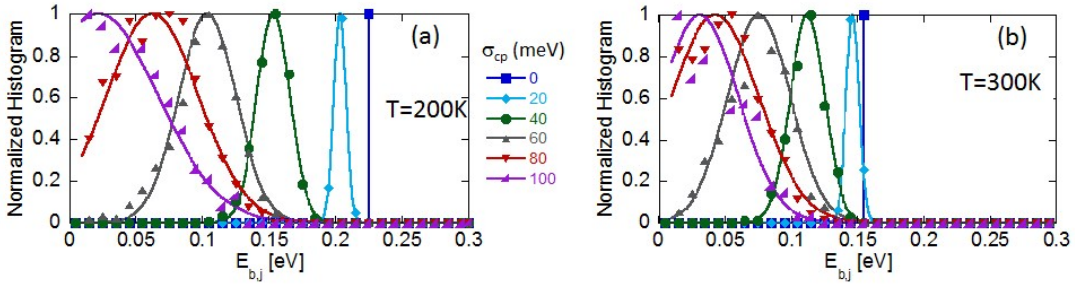

Figure 6S. a) and (b) are the normalized distributions of the local binding energy ($E_{b,j}$) at 200 °K and at 300 °K, respectively. Symbols are the simulation results and solid lines are Gaussian fits. Blue, cyan, green, grey, red, and magenta lines are simulation results for junction disorder standard deviation (σ_{cp}) of 0 meV, 20 meV, 40 meV, 60 meV, 80 meV, and 100 meV, respectively.

4. Dissociation efficiency and binding energy

We have presented a model that accounts for the effect of entropy on CT exciton dissociation in the presence of disorder. Our work builds on the paper by Hood et. al. [1] but the translation of the disordered film to an effective medium is very different. The importance of choosing the most suitable method to "average" the disordered medium to obtain an effective (device equivalent) value has been discussed extensively in the context of charge mobility.[2, 3] Starting our work we could consider three methods of treating entropy and disorder, one of which was used in the main paper. The three methods (Figure 7) start with realizing that the sample should be considered as being composed of different environments (labeled j), each having its own set of disordered energy states and a resulting thermodynamic potential, $\Delta F_j(r)$. The following task is to translate the ensemble of ΔF_j into an effective quantity. The first rigorous treatment of entropy and disorder was by Hood et. al. [1] and in Figure 7 it is depicted as method A. The process of creating the effective, or device equivalent, medium consists of averaging the thermodynamic potentials and using the average potential (ΔF_{eff}) to extract the effective binding energy (see Figure 1 in the main text). The effective binding energy drops to below kT at junction disorder above σ_{cp} = 130meV or bulk disorder of $\sigma_a=\sigma_d$=90meV (Figure 8s). Linking this binding energy to device properties is not straight forward as a binding energy below kT would result in 100% dissociation efficiency regardless of any other material's parameters (as exciton lifetime or charge hopping rate).

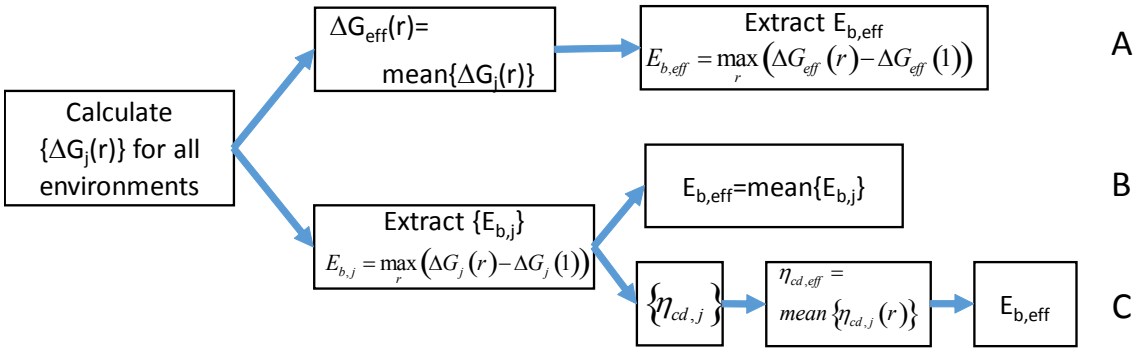

Figure 7S. Illustration of three methods to arrive at an effective binding energy

In Figure 4 we showed that if one does not average ΔF_j but rather extract from every j environment its local binding energy (E_{bj}) and separation distance, than the results have a rather large distribution. As all distributions, in Figure 4, are fitted well by a gaussian it may trigger what we labeled as method B in Figure 7S. Namely, define the effective binding energy as the average, or most probable, binding energy. Using this method, the effective binding energy drops slower, relative to A, as a function of disorder (Figure 8s). However, it also does not lend itself for direct comparison with experimental data. The third method (C in Figure 7) is the one proposed here. The basic idea behind it is to try and mimic the physical process taking place in the solar cell device. Namely, the dissociation efficiency of a device is a result of collecting the charges that were generated at different positions within the layer (i.e. at different environments).

In Figure 8s we compare results obtained by the three methods as well as the effect of the counting strategy. As methods A and B do not provide the effective dissociation efficiency, we compare the binding energies. The top raw of Figure 8s was produced as in the main paper. For each environment to be evaluated, first a 3D lattice of sites energies is generated and then Ω for all 'r' are computed using the same lattice. As the same lattice is used for all 'r' there is some correlation between them. The second and third raw use the method as in ref [1] where for every 'r' one generates a new set of states with their number dictated by the rule ($\Omega=2r^3$ or $\Omega=r^3$).

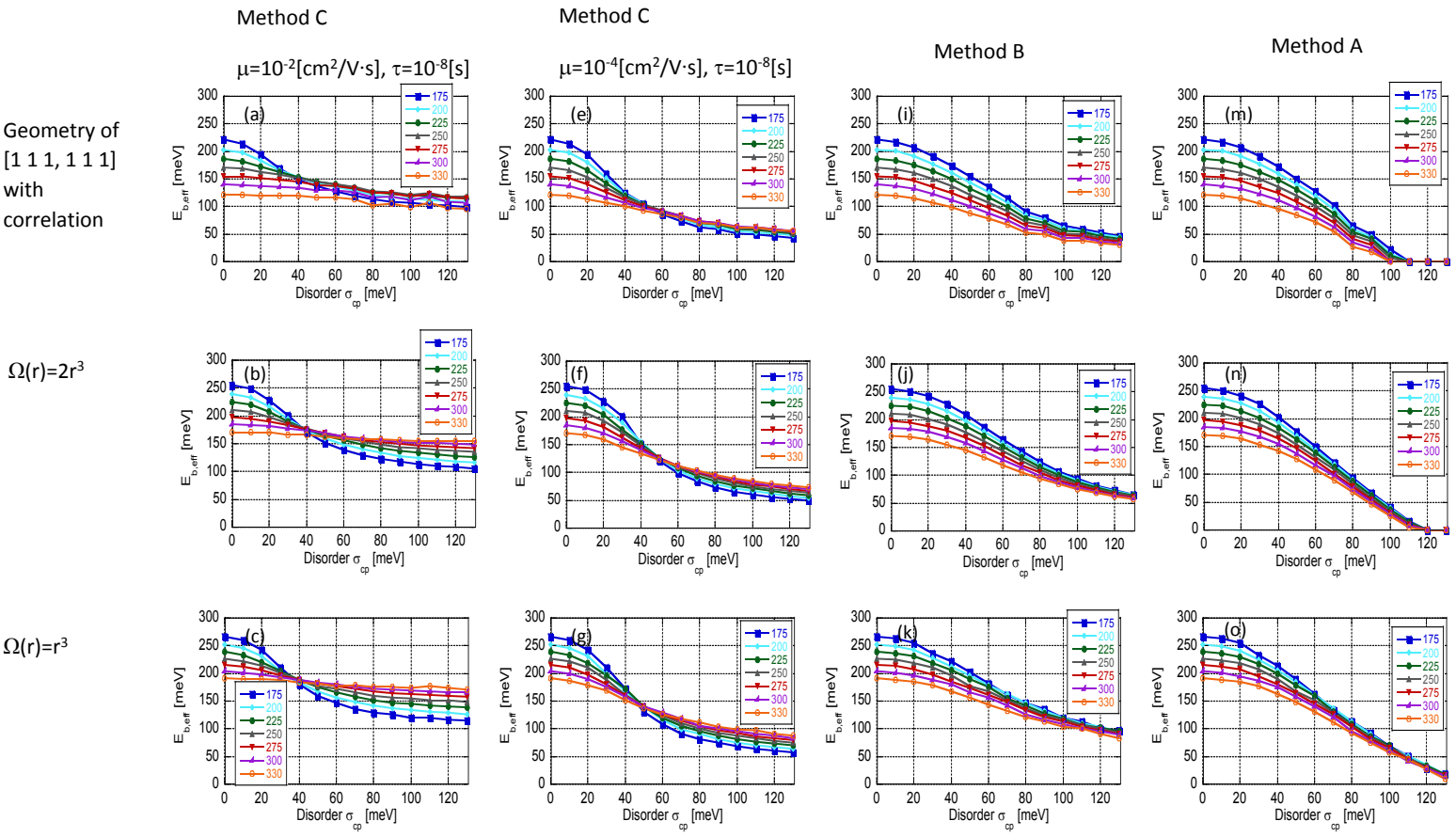

Figure 85. $E_{b,eff}$ *versus disorder for all three methods. (a-c) Method A* $\mu=10^{-2}[cm^2/V\cdot s]$, $\tau_{CT}=10^{-8}[sec]$; *(e-g) Method A* $\mu=10^{-4}[cm^2/V\cdot s]$, $\tau_{CT}=10^{-8}[sec]$; *(i-k) Method B; (m-o) Method C. (a, e, i, m) calculating G(r) while scanning the geometry of [1 1 1, 1 1 1] (with correlation); (b, f, j, n)* $\Omega(r)=2\pi r^3/3$ *no correlation; (c, g, k, o)* $\Omega(r)= r^3$ *no correlation*

First, we discuss differences between results of method A and method B. As long as all CTs dissociate in the same separation distance, method A and B lead to identical results. Thus both methods predict the same $E_{b,eff}$ for low disorder when almost all CT dissociates at the same separation distance. But as the disorder grows, the distribution of dissociation distance becomes wider, each $\Delta F_j(r)$ has maximum at a different r, and by averaging $\Delta F_j(r)$ the maximum value, $E_{b,eff}$, is lowered. Method A produces a fast decreasing $E_{b,eff}$ reaching zero within the disorder range considered. Method B also shows that $E_{b,eff}$ is decreasing, but in a more softened way.

For Method C we use two columns as this method takes into account the materials' physical properties as the exciton lifetime and the mobility (hooping rate). For the two mobilities used we note that the effective binding energy does not reduce to zero. Moreover, at high disorder the temperature dependence flips sign instead of gradually diminishing to zero. The most unique

feature of method C can not be presented in a figure like Figure 8s as it is the only method that directly evaluates the device equivalent effective dissociation efficiency.

5. Further discussion regarding $\eta_{cd,eff}$ and $E_{b,eff}$ dependencies

Figure 9S shows the effective dissociation efficiency at (a) 200[^{0}K] and at (b) 300[^{0}K]. $\kappa_{cd}\tau_{CT}$ range is matched to mobility range of 10^{-5}-10^{-2}[cm^2/V·s], assuming τ_{CT} =10ns. As $\kappa_{cd}\tau_{CT}$ grows, so does the dissociation efficiency as the hopping away (κ_{cd}) becomes faster relative to the decay. In case of ordered or close to an ordered system, the dissociation efficiency is a linear function of $\kappa_{cd}\tau_{CT}$. We may explain this linearity by paying attention to the fact that dissociation rate is respectively low because in the ordered case, unlike the disordered case, all $E_{b,j}$ share almost the same value and it is unlikely to find low $E_{b,j}$. According to eq(11), when dissociation rate is low, $\eta_{cd,eff}$ is a linear function of $\kappa_{cd}\tau_{CT}$:

$$\eta_{cd,eff} = \left\langle \frac{\kappa_{cd}\tau_{CT}\exp\left(-\frac{E_{b,j}}{k_bT}\right)}{\kappa_{cd}\tau_{CT}\exp\left(-\frac{E_{b,j}}{k_bT}\right)+1} \right\rangle_j \xrightarrow[\kappa_{cd}\exp\left(-\frac{E_{b,j}}{k_bT}\right)?\frac{1}{\tau_{CT}}]{} \kappa_{cd}\tau_{CT}\left\langle \exp\left(-\frac{E_{b,j}}{k_bT}\right)\right\rangle$$

The dissociation is more effective as the disorder is increases because the expectation value of $E_{b,j}$ drops as the disorder increases. Naturally, high temperature is another factor that encourages dissociation and leads to high $\eta_{cd,eff}$.

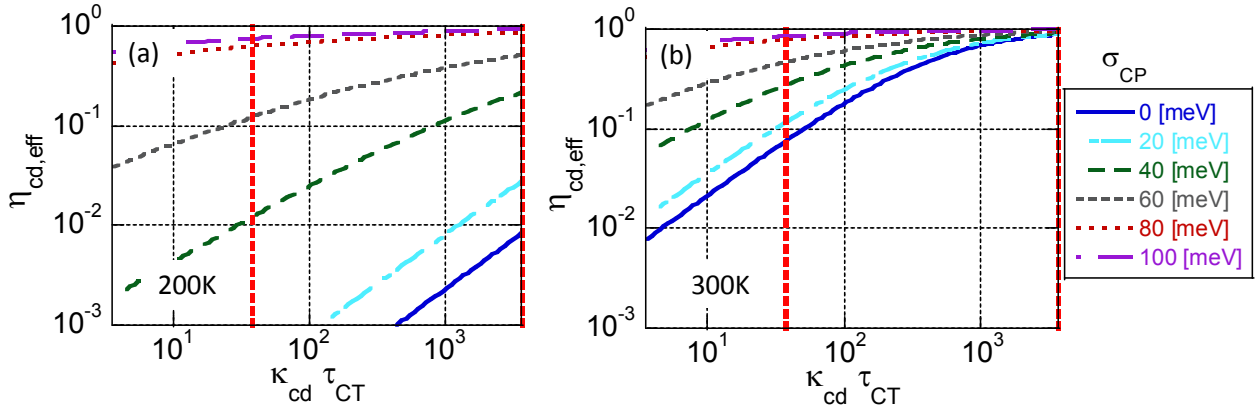

Figure 9S. effective dissociation efficiency ($\eta_{cd,eff}$) as function of $\kappa_{cd}\tau_{CT}$ for various junction disorder standard deviations (a) at 200[K] and at (b) 300[K]. The vertical dashed lines correspond to $\mu=10^{-4}cm^2v^{-1}s^{-1}$ (left line) and $\mu=10^{-2}cm^2v^{-1}s^{-1}$ (right edge line) used for Figure 7 in the main text.

As we deduce $E_{b,eff}$ from $\eta_{cd,eff}$, $E_{b,eff}$ inherits $\eta_{cd,eff}$ temperature, disorder, and $\kappa_{cd}\tau_{CT}$ dependencies. The fact $E_{b,eff}$ is $\kappa_{cd}\tau_{CT}$ dependent shows the insignificance of $E_{b,eff}$ as a key parameter in understanding the dissociation process.

The $\kappa_{cd}\tau_C$ dependence of $E_{b,eff}$ is shown in Figure 10S Again, $\kappa_{cd}\tau_{CT}$ range is matched to mobility range of 10^{-5}-10^{-2}[$cm^2/V{\cdot}s$]. For the ordered case, $E_{b,eff}$ is independent of $\kappa_{cd}\tau_{CT}$ and equals to $E_{b,j}$ which are identical for any j.

It seems that the same conditions which support $\eta_{cd,eff}$ linear dependent on $\kappa_{cd}\tau_{CT}$ are responsible for $E_{b,eff}$ independent of $\kappa_{cd}\tau_{CT}$. We may verify this suspicion by using eq(12) and assuming

$$\eta_{cd,eff} \approx \kappa_{cd}\tau_{CT}\left\langle \exp\left(-\frac{E_{b,j}}{k_bT}\right)\right\rangle_j \quad \text{and } \eta_{cd,eff} \ll 1 \text{(dissociation rate is low):}$$

$$E_{b,eff} = -k_bT\left[\ln\left(\frac{\eta_{cd,eff}}{\left(1-\eta_{cd,eff}\right)}\right)+\ln\left(\frac{k_{decay}}{\kappa_{cd}}\right)\right] \approx -k_bT\left[\ln\left(\frac{\eta_{cd,eff}}{\kappa_{cd}\tau_{CT}}\right)\right] \approx -k_bT\left[\ln\left(\left\langle \exp\left(-\frac{E_{b,j}}{k_bT}\right)\right\rangle_j\right)\right]$$

As $\kappa_{cd}\tau_{CT}$ and disorder are increasing, the assumptions are not holding and $E_{b,eff}$ becomes more

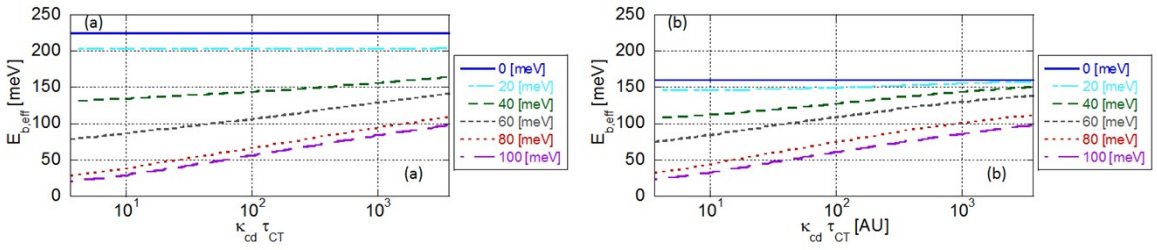

Figure 10S. Effective binding energy as a function of $\kappa_{cd}\tau_{CT}$ for various disorder standard deviations (a) at 200[K] and at (b) 300[K].

$\kappa_{cd}\tau_{CT}$ dependent.

`Figure 9S reveals that as $\kappa_{cd}\tau_{CT}$ is growing, $\eta_{cd,eff}$ tend to unity and all graphs of different disorders are getting closer together. This is the reason for the effect we see in Figure 10S causing all graphs getting closer together as $\kappa_{cd}\tau_{CT}$ increases.

Below we show the same results but where the x-axis is the junction (charge-pair) disorder and the curves are for different charge mobility values (translated to Kcd using Onsager-Braun theory).

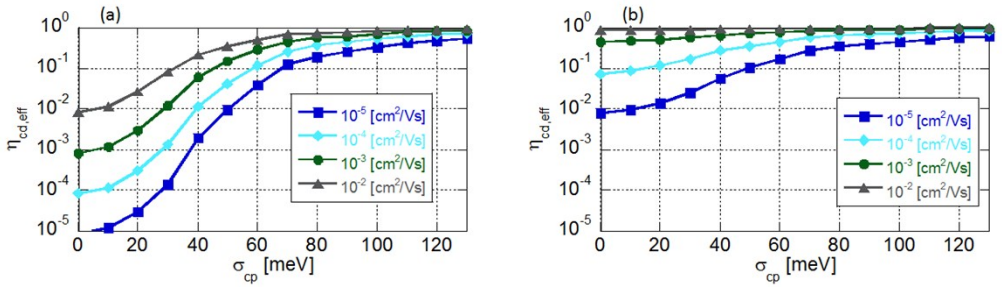

*Figure 11S. effective dissociation efficiency as a function of disorder standard deviation for various values of $\kappa_{cd}\tau_{CT}$ (κ_{cd} values correlates to the mobility values written in the legend, $\tau_{CT}=10^{-8}$[s]) (a) at 200[K] and at (b) 300[K].*at (b)

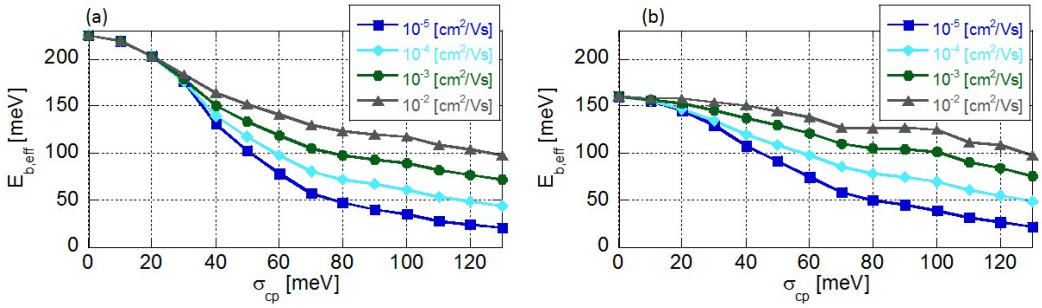

Figure 12S. effective binding energy as a function of disorder standard deviation for various values of (κ_{cd} values correlates to the mobility values written in the legend, $\tau_{CT}=10^{-8}$[s]) (a) at 200[K] and at (b) 300[K].

6. EQE and IQE

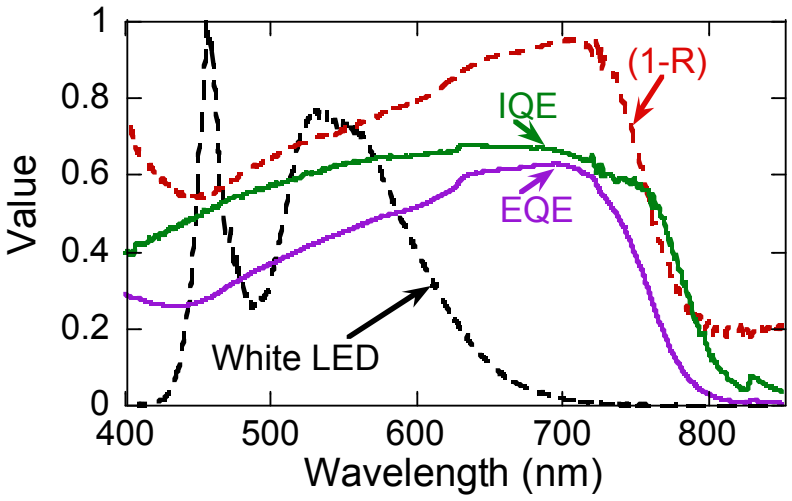

Figure 13s. Spectral distribution of the external quantum efficiency (EQE, purple), internal quantum efficiency (IQE, green), the absorbed fraction as 1 minus the measured cell's reflection (dashed red), the white LED (dashed, black)

The internal quantum efficiency is calculated by dividing the external quantum efficiency (EQE) by the fraction of light absorbed by the cell (1-R).

7. Device simulation data

For parameters we used the effective bandgap of 1.5 eV (deduced from the inset to Figure 6c in main text), disorder parameter for the HOMO and LUMO levels of σ=70 meV, $\mu_e=\mu_h=2\cdot10^{-4}$ $cm^2v^{-1}s^{-1}$, and a low bimolecular recombination of 10^{-12} cm^3s^{-1} (Langevin coefficient is $2\cdot10^{-10}$ cm^3s^{-1}). For the contacts we assumed that the MoO_x has the potential to align with the HOMO level. We used the workfunction of the Zinc Oxide and the trap recombination lifetime (C_pP_T) as fitting parameters to fit the V_{OC} as well as the J-V shape at 1 Sun and 10^{-2} Sun. Best fits (Figure 8 in main text) were achieved using mid-gap traps with recombination lifetime of C_pP_T=8 ns and workfunction of ZnO being 0.22 eV below the LUMO level (of ITIC). Below we add two figures to expand the physical picture captured by the semiconductor device model.

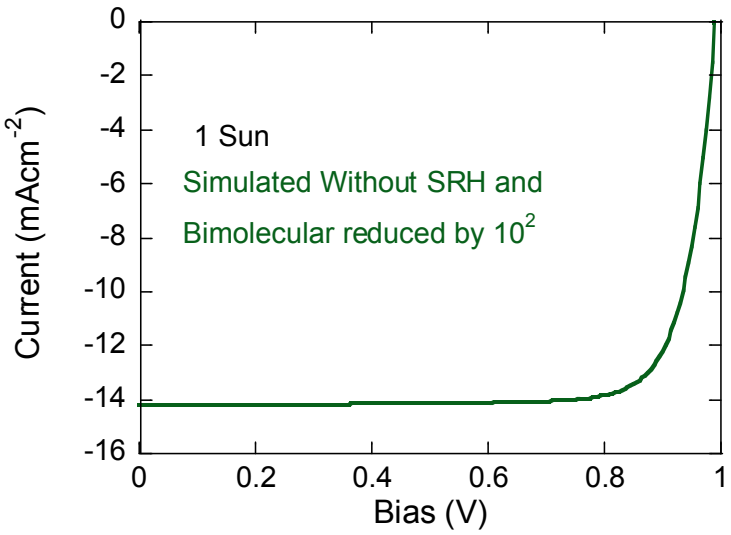

Figure 14s. Simulation of the same device as in the main paper but without trap-assisted recombination and the bimolecular recombination reduced by a factor of 100. The Result indicates that V_OC is limited to below 1V and not by the magnitude of the recombination losses but rather the build in voltage..

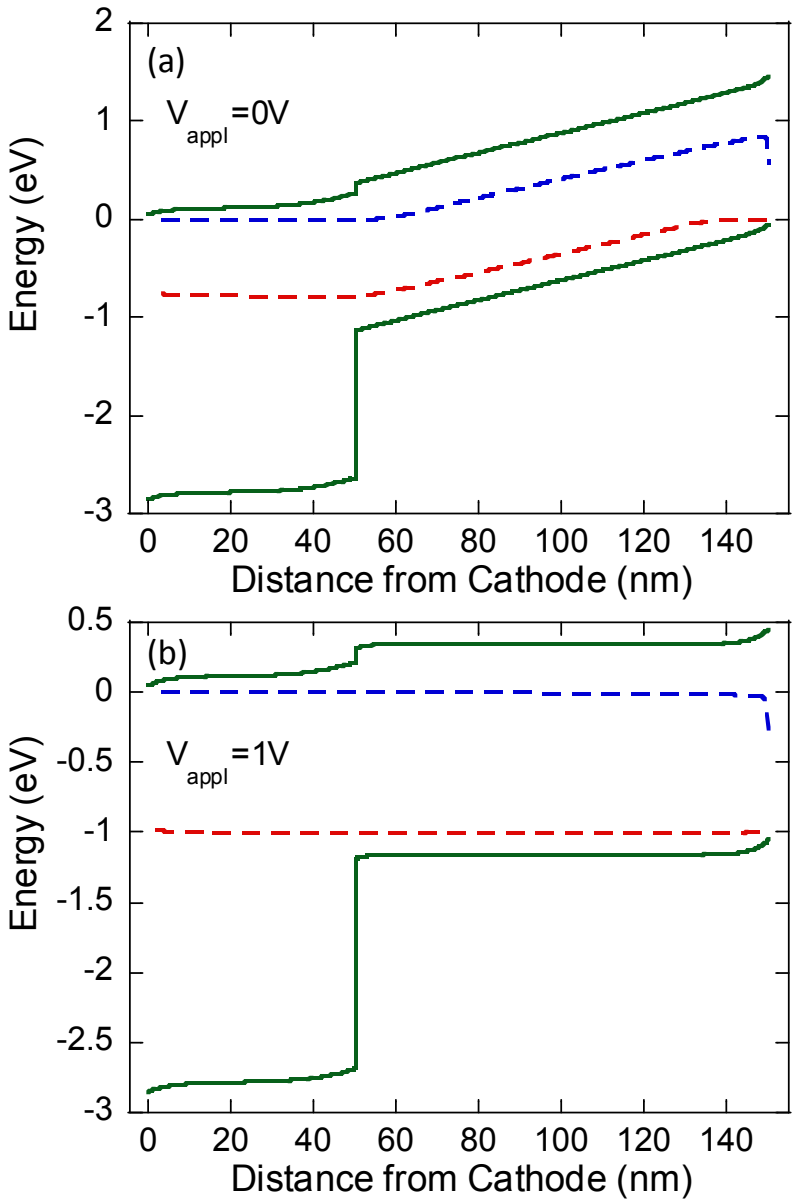

Figure 15s. Band structure of the same device simulated in Figure 14s under 1 Sun excitation. The dashed blue and red lines denote the electron and hole quasi Fermi energy, respectively. (a) at V=0. (b) at V=1V. Note that 1V is the flat band voltage indicating voltage losses at the contacts plus ZnO layer of 0.5V.

References

1. Hood SN, Kassal I. Entropy and Disorder Enable Charge Separation in Organic Solar Cells. *J Phys Chem Lett* 2016, **7**(22)**:** 4495-4500.

2. Tessler N, Preezant Y, Rappaport N, Roichman Y. Charge Transport in Disordered Organic Materials and Its Relevance to Thin-Film Devices: A Tutorial Review. *Adv Mater* 2009, **21**(27)**:** 2741-2761.

3. Baranovskii SD. Theoretical description of charge transport in disordered organic semiconductors. *Phys Status Solidi B-Basic Solid State Phys* 2014, **251**(3)**:** 487-525.